High-strength self-consolidating concrete girders subjected to elevated compressive fiber stresses, part 2: Structural behavior

Jared E. Brewe
and John J. Myers

Editor's quick points

- This paper presents an experimental determination of the flexural and shear behavior of high-strength self-consolidating concrete (HS-SCC) girders subjected to elevated compressive fiber stress levels.
- Experimental results on HS-SCC girders show that actual concrete cracking loads are underestimated by current prediction methods.
- These experimental results also indicate little reduction in flexural capacity of girders subjected to elevated stress levels; however, further testing in shear is needed to reduce the variability in the shear capacity results.

Two goals prompt reconsideration of allowable compressive stress limits for concrete members at release of prestressing: to improve safety by eliminating the need for harping of strands and to increase plant productivity by allowing the release of prestressing at lower concrete strengths. Part 1[1] of this series of papers evaluated allowable compressive stress limits and reviewed their implications for the use of high-strength self-consolidating concrete (HS-SCC) in prestressed concrete members. These issues have attracted significant interest due to their importance for the prestressed concrete industry. Additional background information on this research program is presented in part 1 of this series.

Concrete subjected to high compressive stresses

For ultimate strength, flexural steel reinforcement is located below the neutral axis of a prestressed concrete member. At release of prestressing, the applied prestressing force compresses the bottom fiber, resulting in negative bending. Under service loads, the beam is subjected to positive bending, creating tension on the bottom fiber. If the net result of prestressing and service loading exceeds the tensile strength of the concrete, cracks develop. Typically, under service loads fully prestressed concrete members are designed to prevent cracking, which results in reduced section geometry and can lead to durability problems within the concrete. Therefore, allowable limits exist for the tensile stresses in prestressed concrete members under service loads.

According to research performed by Liniers,[2] the tensile strength of concrete is reduced after concrete is subjected to short-term loading in compression above $0.4 f_{ci}^{'}$. These results indicate that further increasing the fiber stresses above the current allowable $0.6 f_{ci}^{'}$ may result in cracking of prestressed concrete members at reduced levels. It is unclear whether Liniers'[2] work tested normal-strength or high-strength concrete.

Smadi and Slate[3] performed an X-ray investigation of high-strength concrete (HSC) subjected to sustained stress levels from 40% to 95% of ultimate compressive strength. They found that HSC exhibited significantly less microcracking than normal-strength concretes. When cylinders were subjected to sustained loading up to 65% of ultimate strength, HSC had negligible cracking. If the sustained stress was increased to 80%, cracking increased significantly, leading to nonlinear creep behavior. The majority of the cracking below 80% sustained stress consisted of bond cracks between mortar and aggregate.

At a specific section at midspan, the bottom fiber of a prestressed concrete girder is subjected to the highest compressive stress at release and to the highest tensile stress under service loads. To investigate service-load performance, Birrcher et al.[4] investigated the effect of increasing the allowable compressive fiber stress on the cracking moment. They found that current design procedures overestimated the cracking load and that overstressing may result in nonlinear material behavior at service loads. They concluded that increasing the limit to a maximum of $0.70 f_{ci}^{'}$ may be possible; however, full-scale testing is needed to verify the results.

Research program

This research program explored the performance of prestressed concrete girders subjected to elevated compressive fiber stresses at release of prestressing. It was divided into two phases: measurement of time-dependent prestress losses and quantification of structural performance. The first phase was discussed in detail in part 1. It will be summarized as necessary in the following sections. The second phase included flexural and shear testing of the girders. It is discussed here in detail.

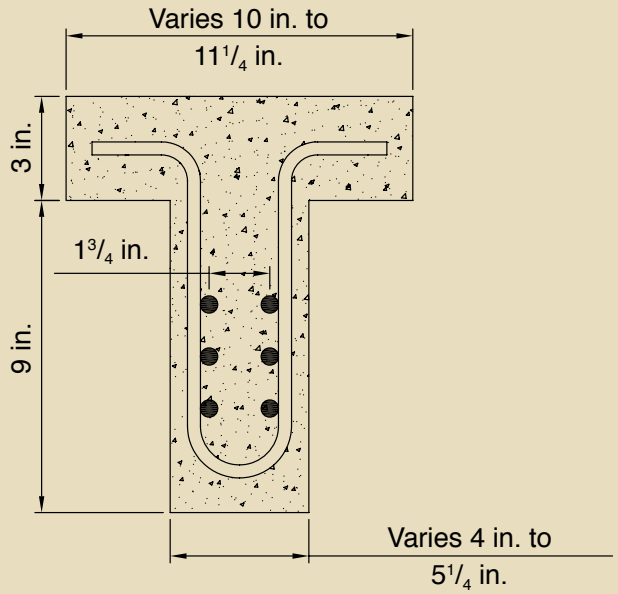

Figure 1. This drawing shows a typical cross section of the girders used in this study. Note: 1 in. = 25.4 mm; 1 ft = 0.305 m.

Six reduced-scale prestressed concrete girders were cast with targeted release stresses from 60% to 80% of the initial concrete compressive strength. Time-dependent prestress losses were measured at regular intervals for 196 days, and the girders were then subjected to structural testing to failure. Three of the girders were designed and tested for flexural behavior. The other three were designed and tested for shear behavior.

Concrete materials

This investigation used an HS-SCC mixture typically specified for transportation projects. The design compressive stresses were 8 ksi (55 MPa) at release of prestressing and 10 ksi (69 MPa) at 28 days. The mixture contained a coarse aggregate content below that normally found in most SCC mixtures, resulting in a reduced modulus of elasticity. Further information about the mixture proportions and constituent materials can be found in part 1.

Girder designs

The girders were designed according to the specifications of the American Association of State Highway and Transportation Officials' *AASHTO LRFD Bridge Design Specifications*,[5] *Building Code Requirements for Structural Concrete (ACI 318-08) and Commentary (ACI 318R-08)*,[6]

Table 1. Beam cross-sectional properties

Girder designation	B-84	B-79	B-75	B-71	B-68	B-65
Target stress level, % of f'_{ci}	80	75	71	68	64	60
Actual stress level, % of f'_{ci}	84	79	75	71	68	65
Gross area of concrete section A_c, in.^{2}	66	69	72	75	78	81
Gross moment of inertia I_g, in.^{4}	855	895	935	975	1014	1053
Distance from CGC to top fiber y_t, in.	4.77	4.83	4.88	4.92	4.96	5.00
Distance from CGC to bottom fiber y_b, in.	7.23	7.17	7.13	7.08	7.04	7.00
Prestressing strand eccentricity e_{ps}, in.	2.73	2.67	2.63	2.58	2.54	2.50
Distance from top fiber to CGS d_p, in.	7.50					

Note: CGC = center of gravity of concrete; CGS = center of gravity of steel. 1 in. = 25.4 mm.

and the *PCI Design Handbook: Precast and Prestressed Concrete*.[7] Compressive fiber stress limits were disregarded. All other specifications, including allowable tension limits, were followed. To simplify fabrication, all six prestressed concrete girders were cast simultaneously on the same prestressing bed. This process produced identical prestressing layouts and jacking levels for every girder, preventing variations in fabrication. **Figure 1** shows a typical girder cross section, and **Table 1** lists cross-sectional properties for all girders.

To achieve higher fiber stresses, the entire section width was reduced in ¼ in. (6 mm) increments, resulting in a reduced area and moment of inertia. This reduction also resulted in greater strand eccentricity, leading to higher stresses. As indicated by the test results, the target compressive strength at release of prestressing was not achieved. Therefore, compressive fiber stresses were higher than anticipated. Thus the label used for each girder in the following discussion corresponds to the actual percentage of concrete fiber stress. Each girder was cast to a length of 15 ft (4.6 m) to ensure full development of prestressing in girders designed for flexural testing.

The flexural reinforcement was designed using strain compatibility with a linear-elastic analysis. As the results indicate, a moment-curvature analysis accounting for nonlinear material behavior is a better predictor of structural performance, but the design used linear-elastic strain compatibility. The resulting longitudinal reinforcement consisted of six ½-in.-diameter (13 mm), low-relaxation prestressing strands. All strands were straight and fully bonded to the concrete, and all had a manufacturer-reported modulus of elasticity of 28,500 ksi (197,000 MPa), conforming to ASTM A416.[8] The strands were jacked to 75% of the ultimate strength by the precast concrete manufacturer, resulting in an initial stress, before any loss, of 202.5 ksi (1396 MPa). Elongation measurements taken before and after jacking were used to determine the initial jacking stress.

The detailed method of analysis given in ACI 318-08 was used for the shear design because of the improved accuracy of the results. The detailed approach accounts for two types of inclined cracking that can result in a shear failure: flexural-shear cracking and web-shear cracking. Flexural-shear cracking occurs after flexural cracking has taken place and can lead to shear-compression failure if not properly reinforced. A shear-compression failure occurs when the compression area at the top of the beam, reduced by diagonal tension cracks, is not sufficient to resist the forces resulting from flexure. Web-shear cracking initiates in the web without flexural cracking and can

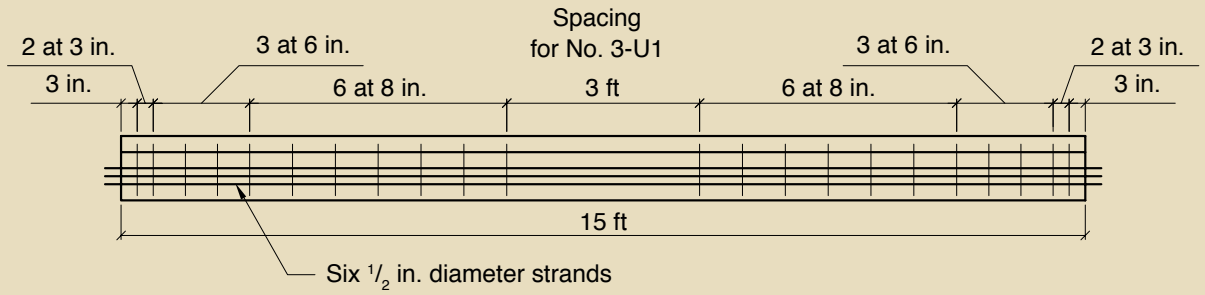

Figure 2. The girders designed for flexural testing had stirrup spacing to prevent shear failure. Note: no. 3 = 10M; 1 in. = 25.4 mm; 1 ft = 0.305 m.

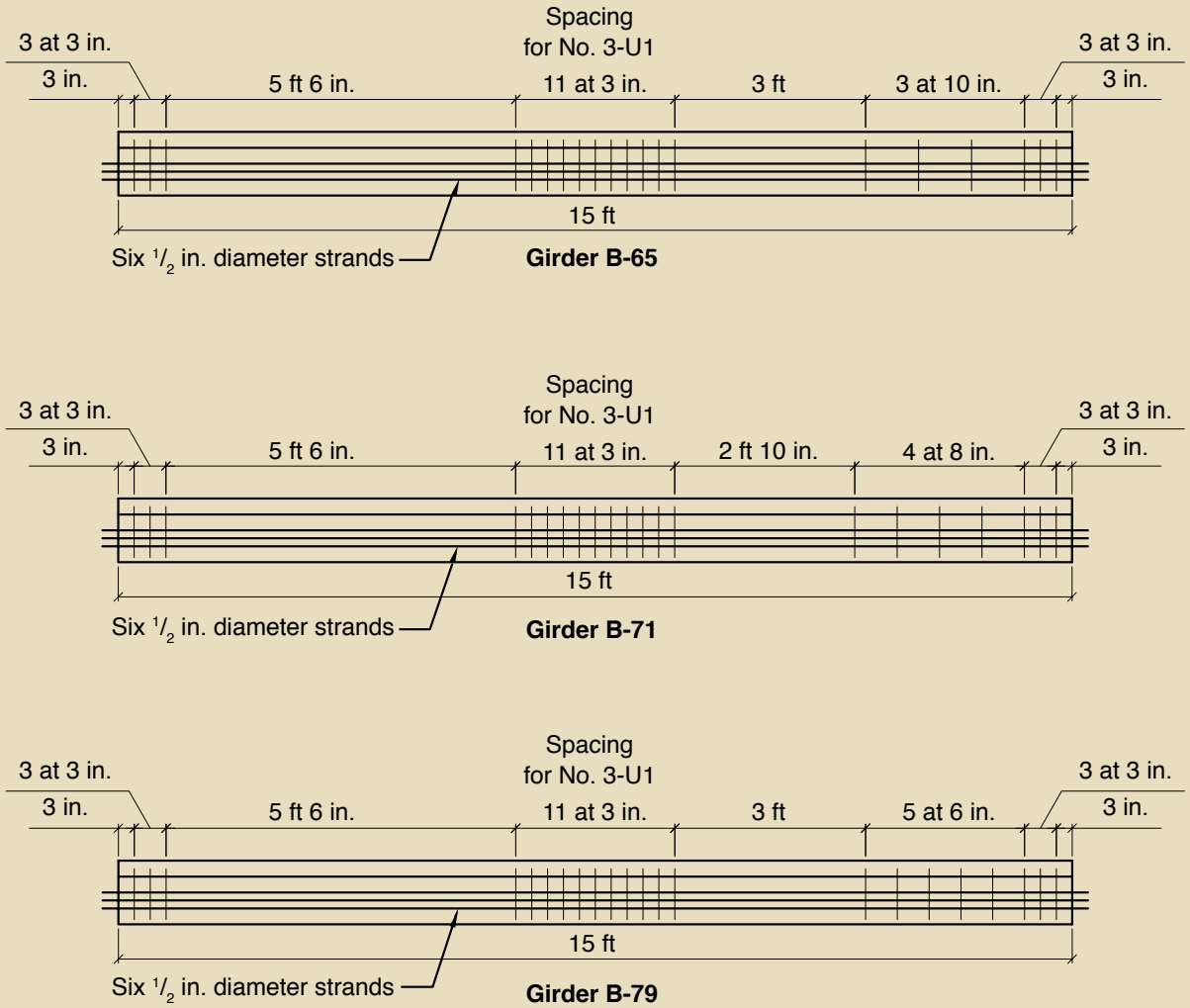

Figure 3. One end of each girder designed for shear testing contained no shear reinforcement, whereas the other end contained stirrups with different spacing. Note: no. 3 = 10M; 1 in. = 25.4 mm; 1 ft = 0.305 m.

occur in thin webs of highly prestressed beams. For simply supported beams, web-shear cracking typically starts below the neutral axis. This type of inclined cracking is less common than flexural-shear cracking. Web-shear cracking occurs when the diagonal (principal) tension stresses reach the tensile strength of the concrete at the center of gravity of the section. Calculations showed that the shear force required to cause flexural-shear cracking was lower than that required to cause web-shear cracking and therefore controlled the design of shear reinforcement.

Transverse shear reinforcement was designed to address the deficiency in shear capacity. Open-ended U-stirrups (Fig. 1) of mild steel conforming to ASTM A615[9] Grade 60 (410 MPa) were provided. The girders designed for flexural testing had stirrup spacing to prevent shear failure (**Fig. 2**). One end of each girder designed for shear testing contained no shear reinforcement, whereas the other end contained stirrups with different spacing (**Fig. 3**). Because this set of girders would be used for two tests, each with a shortened span of 9 ft (2.7 m), additional closely spaced reinforcement was included at midspan to ensure shear failure at the ends. The end with no shear reinforcement was designed to test the contribution of concrete and prestressing to the shear resistance. The other end tested the additional contribution of shear reinforcement.

When high levels of prestress are applied to members, bursting cracks can develop at the ends due to tensile stresses developed within the prestressing strand anchorage zone. These tensile stresses develop perpendicular to the prestressing compressive forces, and when they exceed the tensile strength of concrete, cracks develop. Article 5.10.10.1 of the AASHTO LRFD specifications addresses anchorage zones in pretensioned concrete members. It requires vertical reinforcement in the end zone to provide resistance of at least 4% of the total prestressing force at transfer. The factored bursting resistance of the anchorage zone P_r is calculated from the following equation:

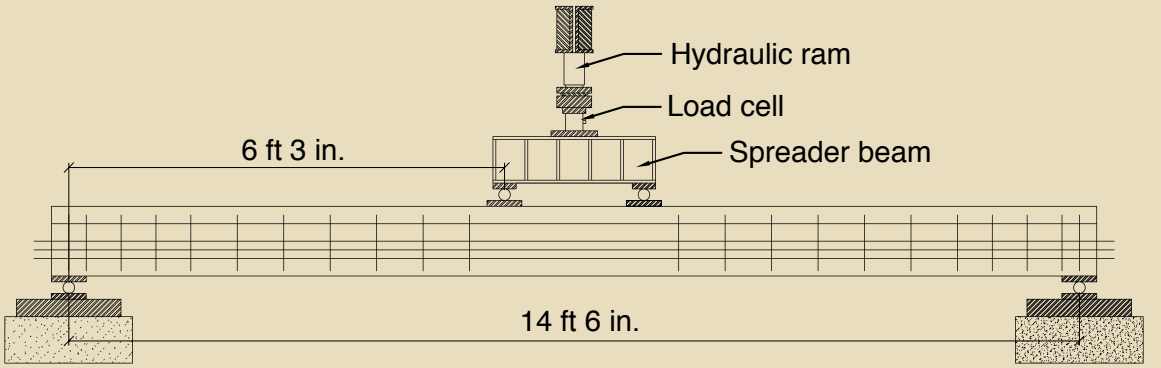

Figure 4. This drawing shows the flexure test setup. Note: 1 in. = 25.4 mm; 1 ft = 0.305 m.

$P_r = f_s A_s$

where

f_s = steel stress for anchorage zone not to exceed a maximum working stress of 20 ksi (137 MPa)

A_s = area of steel to be placed within a distance of $h/4$ from the end of the member (anchorage zone)

h = height of girder

To resist these bursting stresses, an additional stirrup was placed at each end of each girder (Fig. 2 and 3).

Instrumentation

For part 1, concrete surface strains were measured using a detachable mechanical (DEMEC) strain gauge to determine prestress losses. The strains were measured from stainless steel DEMEC target points attached to the girders with commercially available metal/concrete epoxy. The DEMEC gauge has an 8 in. (200 mm) gauge length and is calibrated to measure strain to an accuracy of 8.01×10^{-6} in./in. (mm/mm). The DEMEC target points were placed at regular intervals along the member length and at three different depths along the web section. A more detailed description of the location of the points is provided in part 1.[1]

This portion of work used the DEMEC points placed at different depths near midspan to determine the strain profile under applied loads, which was in turn used to calculate the section curvature and depth to the neutral axis. This calculation provides a check of the theoretical modeling of the member under applied loads. During flexural testing, loading was stopped at regular intervals so that DEMEC measurements could be taken at each level on the three sets of points along the length of the girder.

The load-deformation relationship was measured using a load cell placed under the hydraulic jack, and linear variable differential transformers (LVDT) located at midspan and under each of the applied loads. Concrete surface strains at the top fiber were measured using 2-in.-long (50 mm) strain gauges mounted on concrete epoxy.

Flexure test setup

To develop a constant moment region, the girders were subjected to four-point loading. The supports were located 3 in. (75 mm) from each end of the member. The load was applied with a hydraulic jack located at midspan and separated into two point loads located 12 in. (300 mm) from midspan by a spreader beam. **Figure 4** shows the flexural test setup. The load was applied at an approximate rate of 1000 lb/sec (4.5 kN/sec). Loading was stopped at 10 kip (45 kN), 20 kip (89 kN), and 22.5 kip (100 kN) after flexure cracks became visible and at 30 kip (134 kN) to allow for DEMEC measurements and inspection of cracks. Loading was then applied continuously until failure of the girder.

Shear test setup

For each of the three girders tested in shear, two separate tests were performed. The first test was performed to determine the concrete and prestressing contribution to the shear resistance, and the second test examined the shear reinforcement contribution to the shear resistance. The test setup was nearly identical to the flexure test setup, but the span length was reduced to 9 ft (2.7 m). **Figure 5** shows both shear testing setups. For all tests, the load was applied at a rate of 1000 lb/sec (4.5 kN/sec) until failure. The loading was not stopped at intermediate points because the location of cracking and failure varied for each girder.

Experimental results

Fresh and hardened concrete properties

The fresh and hardened concrete properties were measured according to the applicable standards and guidelines. Con-

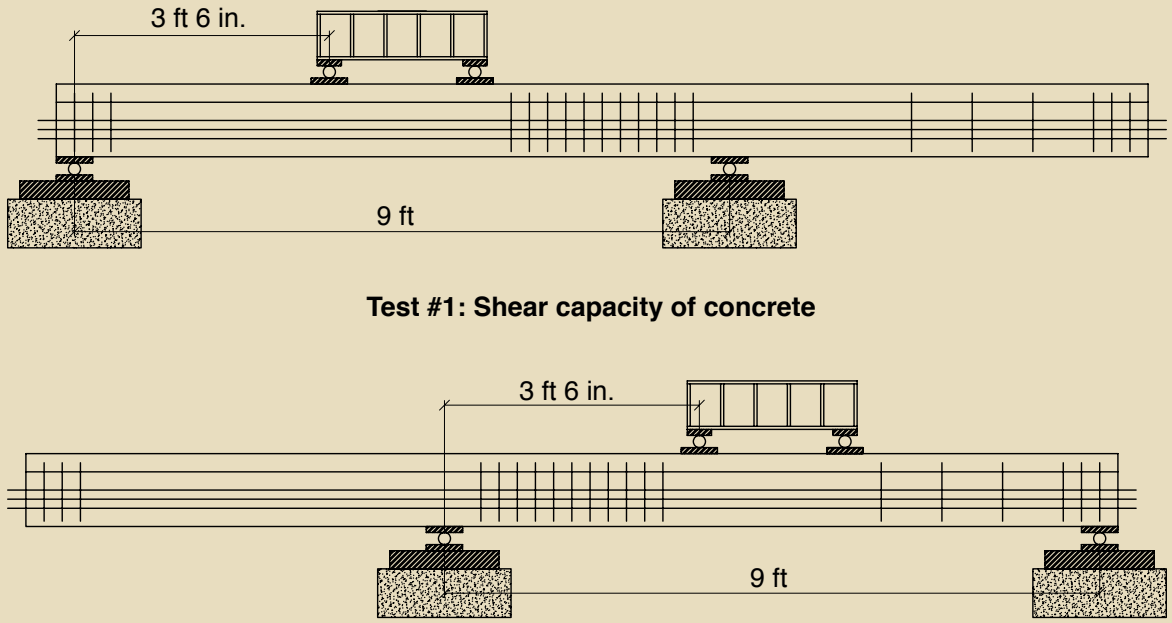

Figure 5. This drawing shows the shear test setup. Note: 1 in. = 25.4 mm; 1 ft = 0.305 m.

Table 2. Measured versus predicted prestress losses at 243 days

Designation		B-84	B-79	B-75	B-71	B-68	B-65
Measured	Loss, ksi	66.5	70.7	64.5	62.9	67.4	57.7
AASHTO LRFD specifications, fourth edition	Loss, ksi	58.7	56.3	54.2	52.2	50.3	48.6
	Difference, %	-12	-20	-16	-17	-25	-16
PCI	Loss, ksi	88.8	84.0	79.7	75.9	72.4	69.2
	Difference, %	33	19	24	21	7	20
AASHTO LRFD specifications, third edition	Loss, ksi	79.3	75.6	72.3	69.3	66.5	64.0
	Difference, %	19	7	12	10	-1	11

Note: 1 ksi = 6.89 MPa.

crete compressive strength at release (3 days) was 7088 psi (49 MPa). The 28-day compressive strength was 9026 psi (62.2 MPa) with a modulus of elasticity of 4635 ksi (31,940 MPa). The concrete strength at 243 days was 8210 psi (57 MPa) with a modulus of elasticity of 4175 ksi (28,785 MPa). The average strength, the coefficient of variation, and the number of concrete cylinder tests at 28 days, 56 days, and 243 days can be found in part 1 along with a discussion of the variations in hardened concrete properties.

Prestress loss behavior

As described in part 1, the development of prestress losses over time was used to determine the effective prestressing force in the strands. These losses were calculated from three concrete surface strain measurements at midspan, averaged to the center of gravity of the steel. Thus the losses were determined from a total of nine measurements. For the purposes of this discussion, **Table 2** presents the total prestress loss measured at test age versus loss calculated by typical prediction methods.

Predicted flexural behavior

For predictions of flexural behavior, several different methods were used to calculate the expected cracking moment (which would be tied to serviceability performance) and the ultimate capacity. The methods used were the *PCI De-*

Table 3. Peak strain values for flexure tests

Designation	B-84		B-75		B-68	
Top fiber strain, × 10^{-6}	-3640	-2954	-2614	-3469	-3232	-2630
Average strain, × 10^{-6}	-3090					

sign Handbook strain compatibility approach, a layer-by-layer moment curvature analysis similar to that described by Collins and Mitchell,[10] and the computer program Response-2000. The moment-curvature and Response-2000 analyses were used to predict the entire load-deformation history. The *PCI Design Handbook* method was used only to determine cracking loads and ultimate capacity.

Accurate determination of the effective prestressing force is essential to determining the cracking load of prestressed girders. Because the effective prestressing force is tied directly to the amount of prestress loss, accurate determination of the losses affects the accuracy of the predictions. Underestimating the prestress loss increases the effective prestressing force, resulting in a predicted cracking load that is higher than that of the actual cracking load for the member. In each of these analyses, therefore, the effective prestressing force was determined by two means: first using the predicted prestress losses determined from the refined estimates method of the AASHTO LRFD specifications and then with the prestress losses measured in phase 1 of this research program. The AASHTO LRFD specifications refined estimates method was selected because it is commonly used throughout the industry. The effective prestressing force has a lesser impact on the ultimate capacity because it is determined when the materials fail.

The *PCI Design Handbook* predicts the cracking moment M_{cr} using the following equation:

$$M_{cr} = P_{eff} e_{ps} + \frac{P_{eff} S_b}{A_c} + f_r S_b$$

where

P_{eff} = effective prestressing force after losses

e_{ps} = prestressing strand eccentricity

S_b = gross bottom-section modulus

A_c = gross concrete-section area

f_r = modulus of rupture of concrete, which was assumed to be 7.5 times the square root of the compressive strength of concrete as defined in the handbook

Like the modulus of elasticity, the modulus of rupture is sensitive to the constituent materials. This value was developed from data on conventional and high-strength concrete, but without additional data on SCC it is assumed to be valid.

The moment is converted to two equivalent, equally spaced point loads using the following equation:

$$P = \frac{2\left(M - M_d\right)}{a}$$

where

P = applied load

M = applied moment

M_d = dead-load moment

a = distance between the support and the concentrated load

The ultimate flexural capacity was calculated using the strain compatibility method because the *PCI Design Handbook* notes that this method is typically more accurate than standard code equations. The effective strain in the top fiber at failure was assumed to be 0.003 in./in. (mm/mm). This correlates well with the average strain value of 0.00309 in./in. (mm/mm), measured using two strain gauges mounted on top of each girder during loading (**Table 3**). The effective prestress was determined for each individual layer, and standard principles of mechanics were used to determine the ultimate flexural capacity. Using these values, the ultimate load was determined from the previous equation.

Moment-curvature analysis was chosen to predict behavior because it has been widely used to analyze structures. Moment-curvature analysis provides a more detailed and accurate prediction of the deflection and flexural capacity of a member and explains the behavior of the member in progressive loading stages leading to failure. This method develops a rational analysis that follows the behavior of the bonded prestressed concrete beam through the total load range from initial loading to the failure stage. To improve the results, analysis was performed using the layer-by-layer method, dividing the cross section into several layers. The top-fiber strain in the concrete and the position of the neutral axis are assumed to obtain the concrete strain distribution. The stress-strain profile used for concrete was the relationship developed by Thorenfeldt et al., while the modified Ramberg-Osgood function was used for the prestressing.[10] Prior to concrete cracking, the moment-cur-

vature analysis produces results similar to the behavior predicted by the *PCI Design Handbook* method because the girders are assumed to remain linear elastic. Post-cracking response was determined using the layer-by-layer method, and the resultant concrete compressive stress C_c was found using the following equation:

$$C_c = \sum A_{ci} f_{ci}$$

where

A_{ci} = area of each individual concrete layer

f_{ci} = stress at the centroid of each individual concrete layer determined from the calculated strain and Thorenfeldt's equation

The resultant steel tensile stress T_s was calculated using the following equation:

$$T_s = \sum A_{ps} f_{pe}$$

where

A_{ps} = area of each layer of prestressing tendons

f_{pe} = effective prestress after losses

Therefore, for a given top-fiber strain, the depth to the neutral axis can be found when the resultant concrete stress is equal to the steel stress. The moment is found by multiplying each resultant force with the distance to the neutral axis and adding the results. The corresponding curvature can be calculated by dividing the strain in the top fiber by the depth to the neutral axis. Increasing the assumed top-fiber strain results in increased force resultants and moments, which are used to develop the moment-curvature response. The calculated moments were translated into load using the earlier equation. The conjugate beam method was used with numerical integration to calculate the girder deflections from the curvature along the member:

$$\Delta = \left(\frac{\phi_1 x_1 + \phi_2 x_2}{2}\right)\Delta x_1 + \left(\frac{\phi_2 x_2 + \phi_3 x_3}{2}\right)\Delta x_2 + \ldots$$

where

Δ = midspan displacement

ϕ = curvature at a specific point x

Δx = distance between two points

The computer program Response-2000 performs calculations similar to those involved in moment-curvature analysis. The analyses produced slightly different predictions of elastic behavior because the computer program included the effect of tension stiffening in the post-cracking response.

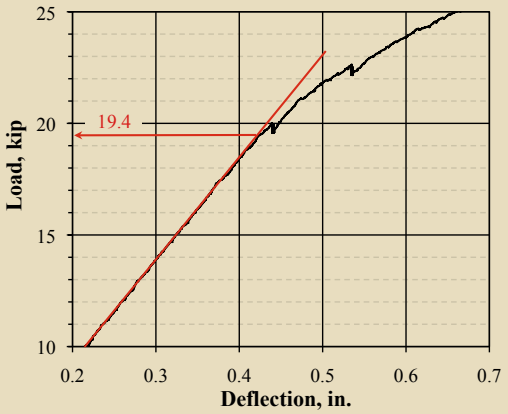

Figure 6. This figure demonstrates the method used to determine the approximate cracking load for girder B-84. Note: 1 in. = 25.4 mm; 1 kip = 4.448 kN.

Flexure results

In reinforced concrete or prestressed concrete, flexural cracks form when the tensile stress in the bottom fiber of the member exceeds the modulus of rupture of the concrete. Prior to this point, the member behaves in a linear-elastic fashion according to Hooke's law. Therefore, the cracking load can be determined from the load-deformation plot when that relationship no longer appears linear. **Figure 6** demonstrates the method used to determine the approximate cracking load for girder B-84, with a similar method employed for girders B-75 and B-68. As an alternative to estimating from the plots, the cracking load can also be approximated from the strain measured using the DEMEC points mounted on the sides of the girders. Because the loading was stopped at 10 kip and 20 kip (44.5 kN and 89 kN) and given that the strain was assumed to have a linear distribution, the strain at the bottom fiber can be extrapolated from the measurements. Using those data points, the cracking load could be estimated by interpolating between 10 kip and 20 kip (44.5 kN and 89 kN) until the bottom fiber strain equaled the strain at the modulus of rupture. As a result, the values estimated from the plots and those determined from the strain profile were in relatively close agreement.

Table 4 lists the estimated cracking loads for the three girders, the comparison of cracking loads predicted by the three methods described above with the actual cracking loads, and the ratio of the predicted cracking load to the measured cracking load. The effective prestressing force has a significant impact on the predicted cracking load. Therefore, the predicted cracking loads were calculated using both predicted prestress losses and measured prestress losses. The ratios show that all three methods, using both predicted and measured losses, underestimated

Table 4. Comparison of actual versus predicted cracking load for flexure tests

Designation	B-84		B-75		B-68	
Actual cracking load, kip	18.5	Ratio*	19.1	Ratio*	19.4	Ratio*
Predicted cracking load using predicted losses						
PCI Design Handbook, kip	17.2	0.93	16.7	0.87	18.0	0.93
Moment-curvature analysis, kip	18.1	0.98	18.5	0.97	18.8	0.97
Response-2000, kip	16.6	0.90	17.2	0.90	17.6	0.91
Predicted cracking load using measured losses						
PCI Design Handbook, kip	16.6	0.90	16.9	0.88	16.5	0.85
Moment-curvature analysis, kip	17.4	0.94	17.5	0.92	17.3	0.89
Response-2000, kip	16.0	0.87	16.4	0.86	16.2	0.83

*Ratio of predicted cracking load to measured cracking load.
Note: 1 kip = 4.45 kN.

the cracking load by about 16%. Such underestimation results in a conservative prediction of member behavior. Birrcher et al. performed a similar analysis on HSC girders subjected to elevated compressive fiber stresses at release. They found that the procedure outlined in the *PCI Design Handbook* and the *AASHTO LRFD Bridge Design Specifications—2005 Interim Revisions*[11] for prediction of prestress losses and cracking loads overestimated the actual cracking load. The *PCI Design Handbook* method overestimated the cracking load by an average of 10.2%, with a high of 22.5%, and the AASHTO LRFD specifications 2005 interim revisions overestimated the cracking loads by an average of 4.4%, with a high of 13%. Because the calculated cracking load is based on estimated prestress losses, the accuracy of the predicted capacity depends on the accuracy of those loss estimations.

Figures 7, **8**, and **9** show the complete load-deflection relationships for girders B-84, B-75, and B-68, respectively. These figures also show the predicted response according to the moment-curvature analysis and Response-2000. They demonstrate that the author-developed moment-curvature analysis is a better predictor of linear-elastic behavior, whereas Response-2000 better predicts inelastic behavior because the software considers tension stiffening in its calculations. **Table 5** shows predicted and measured ultimate moment capacity and the ratio of the predicted-to-measured ultimate capacity for all three girders. This

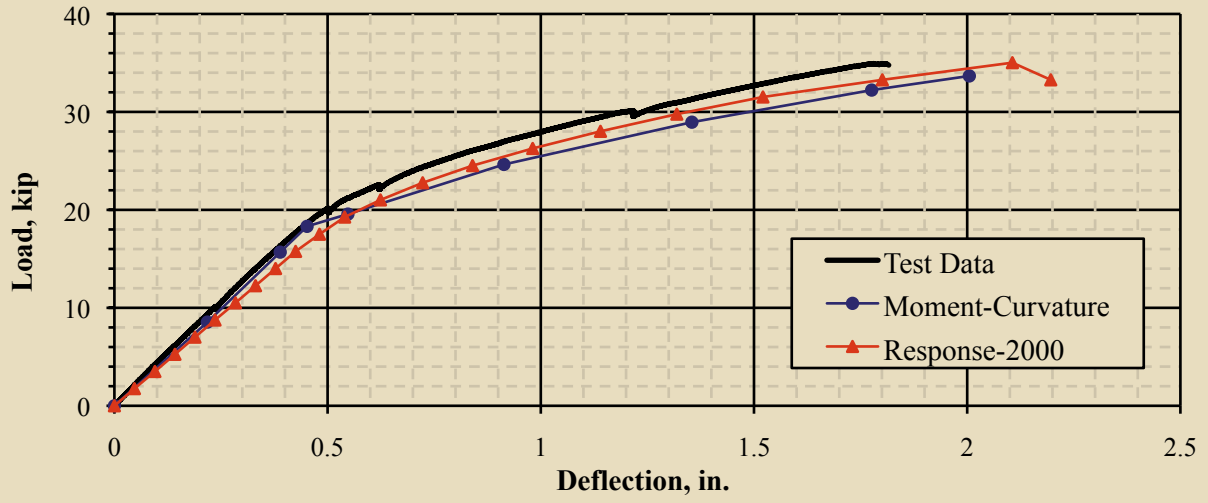

Figure 7. This figure shows the complete load-displacement relationship for girder B-84 and the predicted response according to the moment-curvature analysis and Response-2000. Note: 1 in. = 25.4 mm; 1 kip = 4.448 kN.

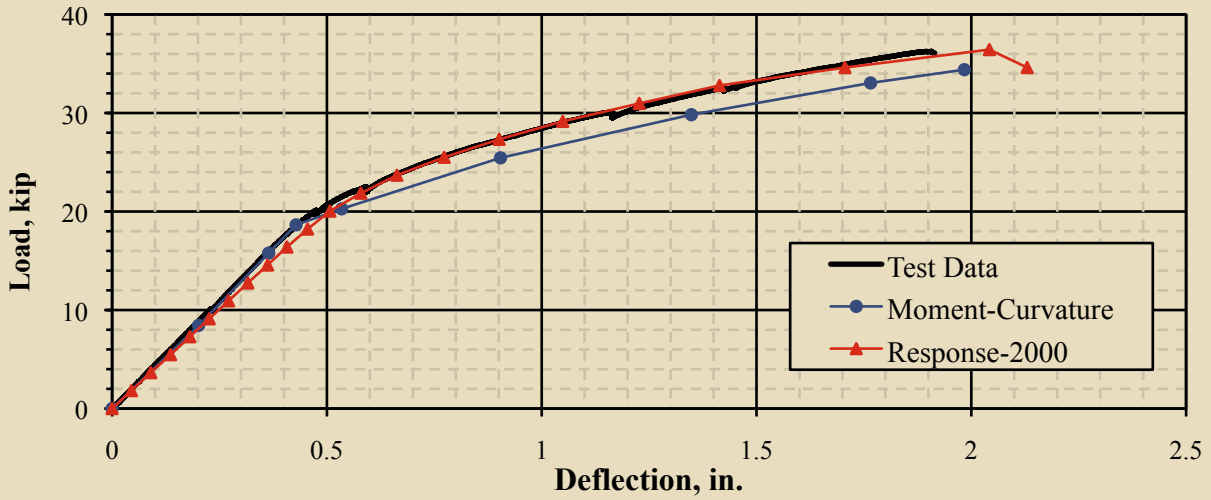

Figure 8. This figure shows the complete load-displacement relationship for girder B-75 and the predicted response according to the moment-curvature analysis and Response-2000. Note: 1 in. = 25.4 mm; 1 kip = 4.448 kN.

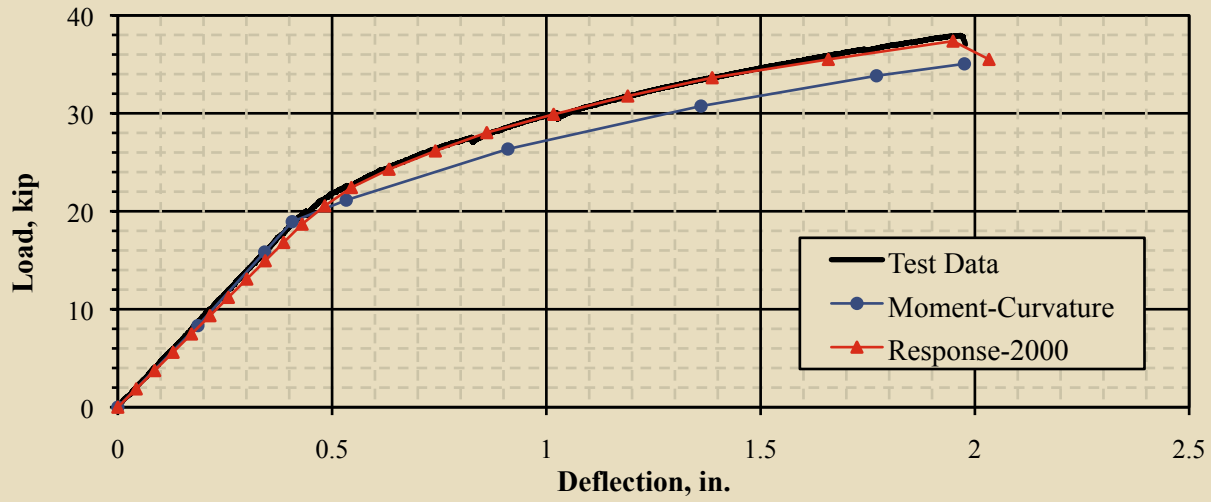

Figure 9. This figure shows the complete load-displacement relationship for girder B-68 and the predicted response according to the moment-curvature analysis and Response-2000. Note: 1 in. = 25.4 mm; 1 kip = 4.448 kN.

indicates that each method predicts the ultimate capacity to within 14% of the calculated capacity, improving the accuracy with more advanced analysis.

Similar to the cracking load, ultimate capacity is also underestimated by all three prediction methods, leading to conservative predictions. The difference between calculated ultimate capacity based on predicted losses and that based on measured losses demonstrates that variations in the effective prestressing force have a relatively small impact on predictions of ultimate capacity.

The displacement of members subjected to bending depends on the stiffness of the member, specifically the inverse of the stiffness. The member stiffness is determined from the modulus of elasticity of the material and the moment of inertia. Because all girders were cast simultaneously, the modulus of elasticity is assumed to be uniform among them. Thus, the only difference is the geometrical properties of the members. Therefore, normalization can permit comparison of the load-displacement relationship for members of various sizes. **Figure 10** presents the load-displacement relationship for all three girders normalized to the stiffness of girder B-68. It indicates that the relative

Table 5. Comparison of actual versus predicted ultimate load

Designation	B-84		B-75		B-68	
Actual failure load, kip	34.9	Ratio*	36.3	Ratio*	38.0	Ratio*
Predicted failure load using predicted losses						
PCI Design Handbook, kip	31.4	0.90	32.5	0.90	33.5	0.88
Moment-curvature analysis, kip	32.4	0.93	33.2	0.91	34.0	0.90
Response-2000, kip	33.9	0.97	35.1	0.97	36.1	0.95
Predicted failure load using measured losses						
PCI Design Handbook, kip	31.1	0.89	32.1	0.88	32.7	0.86
Moment-curvature analysis, kip	32.0	0.92	32.9	0.91	33.5	0.88
Response-2000, kip	33.9	0.97	34.7	0.96	35.6	0.94

*Ratio of predicted capacity to measured capacity
Note: 1 kip = 4.45 kN.

flexural behavior of each girder is similar except for the capacity of the member, which depends on the width of the compression block.

Predicted shear behavior

The behavior of members subjected to shear is not as well understood as that of members subjected to flexure. The predicted behavior of flexural members follows conventional principles of material properties and strain compatibility, whereas shear capacity has traditionally been predicted using empirical relationships.

Both AASHTO LRFD specifications and ACI 318-08 use empirical equations to determine the contribution of concrete shear capacity, whether prestressed or nonprestressed, to the total shear capacity of the member. Because the shear capacity of concrete is closely related to the mixture proportions, and especially to the coarse aggregate content, empirical equations developed for normal-strength concrete may not apply to high-strength or self-consolidating concrete. In this project, the shear capacity was determined using the detailed method outlined in ACI 318-08 and discussed in the *PCI Design Handbook*. For the girder ends without shear reinforcement, the expected capacity was calculated from the limiting value of web-shear and flexure-shear cracking. For all three girders, flexure shear was found to be deficient in an area approximately 12 in. (300 mm) wide next to the applied concentrated load. For the girder ends with stirrups, the shear capacity was smaller in the same area next to the support but had a larger value due to the contribution from shear reinforcement. The

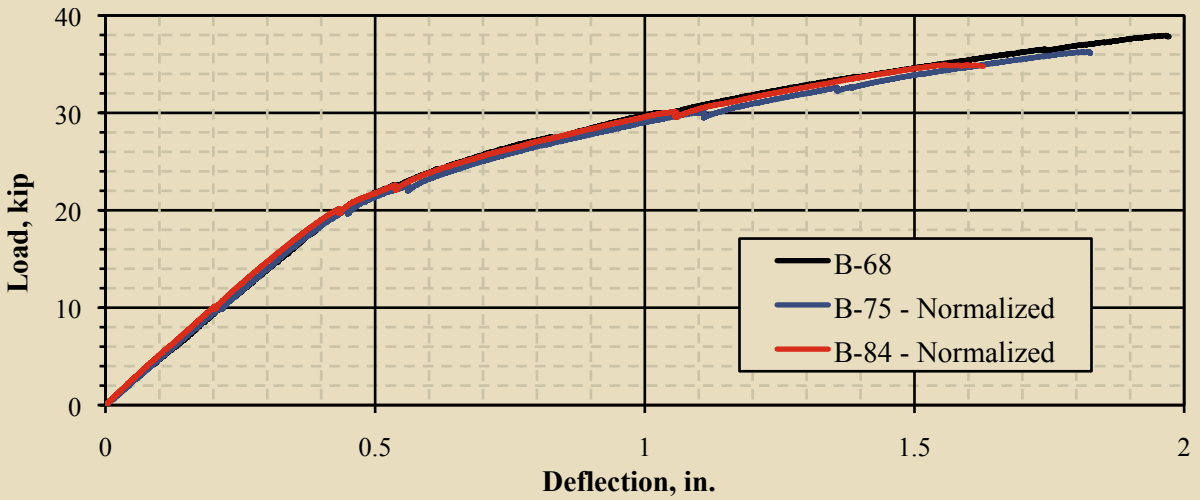

Figure 10. This figure presents the load-displacement relationship for all three girders normalized to the stiffness of girder B-68. Note: 1 in. = 25.4 mm; 1 kip = 4.448 kN.

contribution to shear capacity from the shear reinforcement was determined according to ACI 318-08 section 11.5.7.2, which assumes that cracks are inclined at 45 deg.

The computer program Response-2000 predicts shear capacity based on the modified compression field theory and was used to analyze the girders with and without shear reinforcement. The program calculates the capacity at various sections along the girder length and determines the minimum load causing failure.

Shear results

The typical method used to visualize shear behavior is the plot of shear force (or stress) versus shear strain. The shear force was easily determined from load tests because it is equal to the applied load. The shear strain, however, was not as easy to measure because the location of shear failure (that is, the point where the shear strain was greatest) occurred at varying points along the girders. For simplicity and to maintain uniformity with the flexural tests, the shear behavior was plotted as the relationship between applied load (shear) and displacement at the point of load.

Bursting cracks developed at the ends of the girders, reducing the shear capacity of some girders. As noted previously, the design of prestressed concrete members must be checked to control high tensile forces that develop perpendicular to the prestressing strands that often lead to cracking. For this set of girders, cracking did not occur instantaneously with the release of prestressing. Rather, cracks developed as concrete shrinkage and creep added additional stresses. On 7 of the 12 girder ends, these cracks occurred at one level of prestressing and extended in from the end between 6 in. and 18 in. (15 mm and 46 mm). The cause of these cracks was most likely the increased level of prestressing applied to achieve the high fiber stresses required by the research program. These bursting cracks did not influence the flexural behavior, but they did appear to contribute to a reduction in shear capacity.

Figures 11, **12**, and **13** show the load-displacement relationships for girders B-79, B-71, and B-65, respectively, both with and without shear reinforcement. In each of these figures, the point where the load-displacement relationship is no longer linear signifies development of shear cracks within the girders and the transfer of shear to the transverse reinforcement. This point corresponds to a value slightly larger than the shear capacity of the concrete because some of the shear force is already transferred to the transverse reinforcement. **Figure 14** compares the load-displacement relationship for the ends of the girders without shear reinforcement, and **Fig. 15** compares the relationship for the ends of the girders with shear reinforcement. Both figures indicate little difference in behavior aside from the differing amounts of shear reinforcement.

Figure 16 shows the crack patterns of each of the failed tests. The bursting cracks are visible, and their influence on the failure of the girders is apparent. When the bursting cracks extended well into the girder, the shearing forces widened them, and the failure extended from them. In girders without shear reinforcement, cracks developed beside the support and extended directly to the point of applied load, similar to a deep beam behavior with a direct compression strut. The cracking was typically initiated in the web, indicating web-shear failure, which does not match the design calculations. Due to the small inclination (less than 16 deg) of the compression strut and the reinforcement configuration, a strut-and-tie model produced unreli-

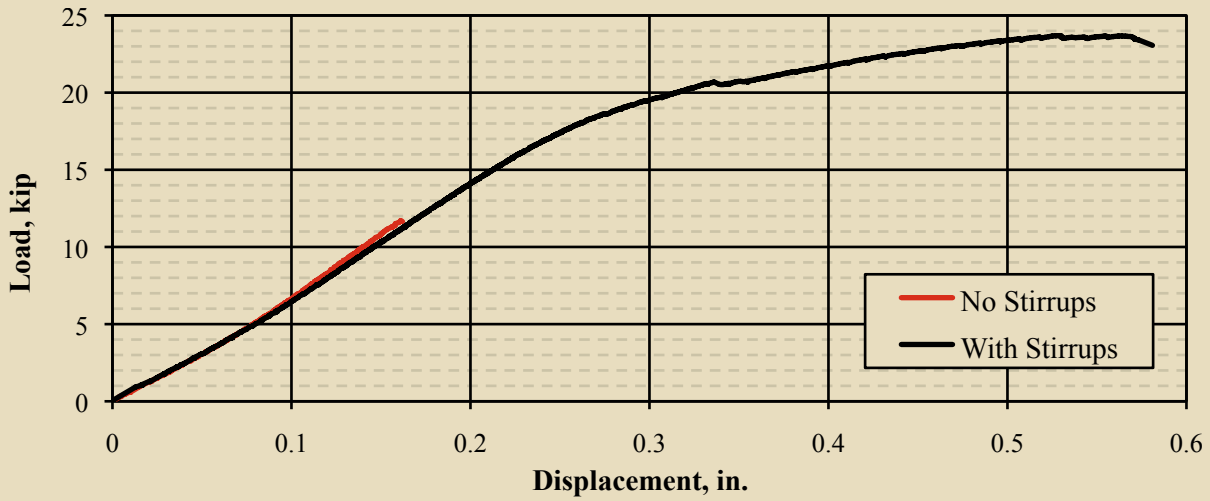

Figure 11. This graph shows the shear behavior of girder B-79. Note: 1 in. = 25.4 mm; 1 kip = 4.448 kN.

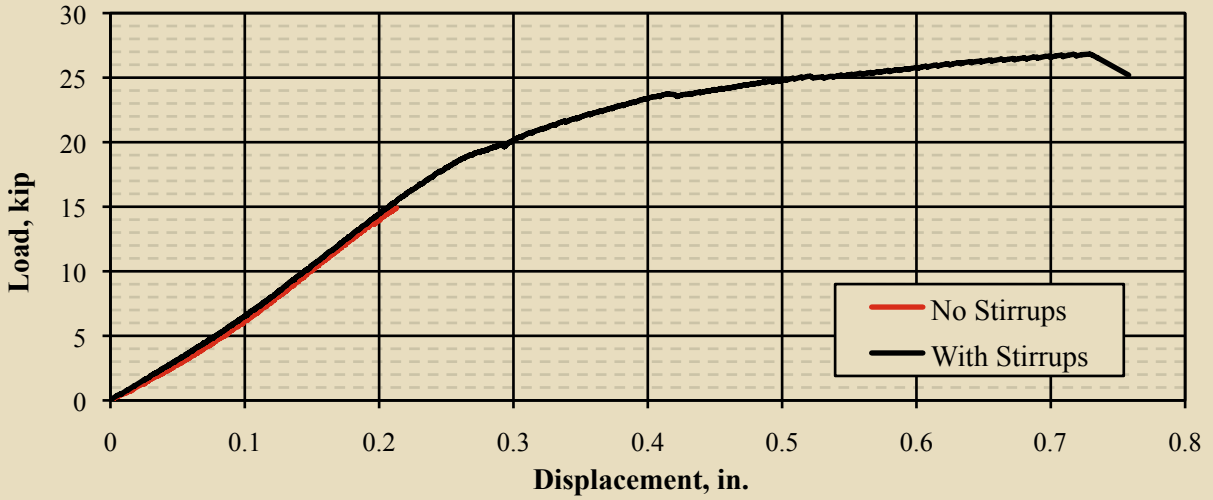

Figure 12. This graph shows the shear behavior of girder B-71. Note: 1 in. = 25.4 mm; 1 kip = 4.448 kN.

able results. In girders with shear reinforcement, flexure cracks developed first, followed by shear cracking through a stirrup, indicating flexure-shear failure as predicted. The crack inclination on these members was about 45 deg, as assumed in the design equation.

Table 6 lists the measured shear capacity with the predicted shear capacity outlined previously for the ends without shear reinforcement and presents the ratio of the predicted to measured capacity. **Table 7** presents a similar comparison for the ends with reinforcement. Both tables indicate that shear failure occurred below the predicted shear capacity in nearly every test. The only underestimation of capacity occurred using the *PCI Design Handbook* method on girder B-65, with an error of 11.6%. For the remaining predictions, the error ranged from 2.4% to 99% overestimation. Test results reported by Naito et al.[12] showed similar behavior in girders produced with SCC and those produced with high-early-strength concrete, with actual capacity exceeding predicted capacity. These results and the failure patterns (Fig. 18) indicate that to ensure adequate safety, additional testing is needed for girders produced using normal- and higher-strength SCC with lesser coarse aggregate contents.

Conclusion

Numerous factors affect the structural performance of prestressed concrete members, especially the concrete proper-

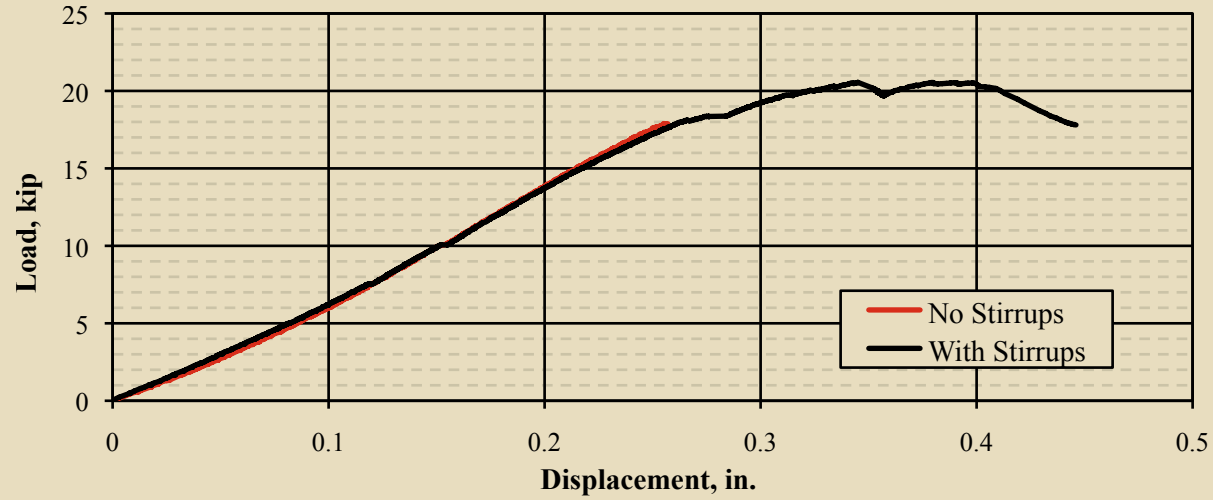

Figure 13. This graph shows the shear behavior of girder B-65. Note: 1 in. = 25.4 mm; 1 kip = 4.448 kN.

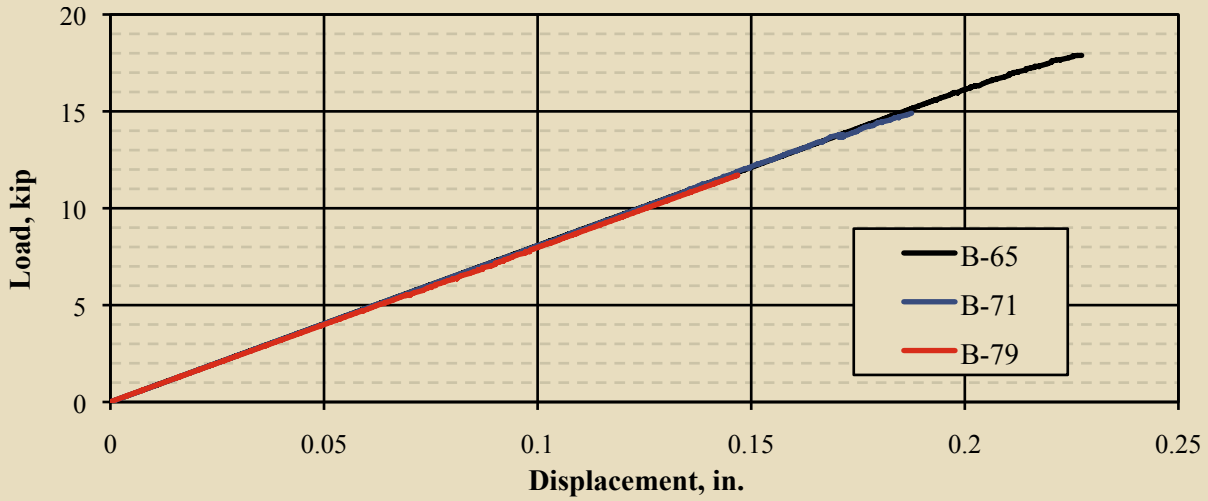

Figure 14. This figure compares the load-displacement relationship for the ends of the girders without shear reinforcement. Note: 1 in. = 25.4 mm; 1 kip = 4.448 kN.

ties. The results of the experimental program described here, along with the results from phase I of this research program on prestress losses, suggest the following:

- Self-consolidating concrete produced with lower coarse aggregate contents reduces the modulus of elasticity of the concrete. Further investigation is needed to determine the effect of reduced modulus-of-elasticity values on the overall performance of prestressed concrete.
- The methods presented here for predicting the cracking load are conservative when compared with experimental results. All of these methods underestimated the cracking load by about 16% of the measured value.
- The methods presented in the paper also provide conservative predictions of the ultimate flexural capacity of the section. All methods underestimated the capacity by 14% of the actual capacity.
- Increasing the fiber stress level at release of prestressing to at least $0.70 f_{ci}'$ appears feasible, as indicated by the work presented here and performed by others as discussed in part 1. Following the change of allowable compressive stress at the ends included in ACI 318-08, an increase in the allowable stress limit to at least $0.70 f_{ci}'$ at any point along the member should be considered for ACI 318-08 and AASHTO LRFD specifications.

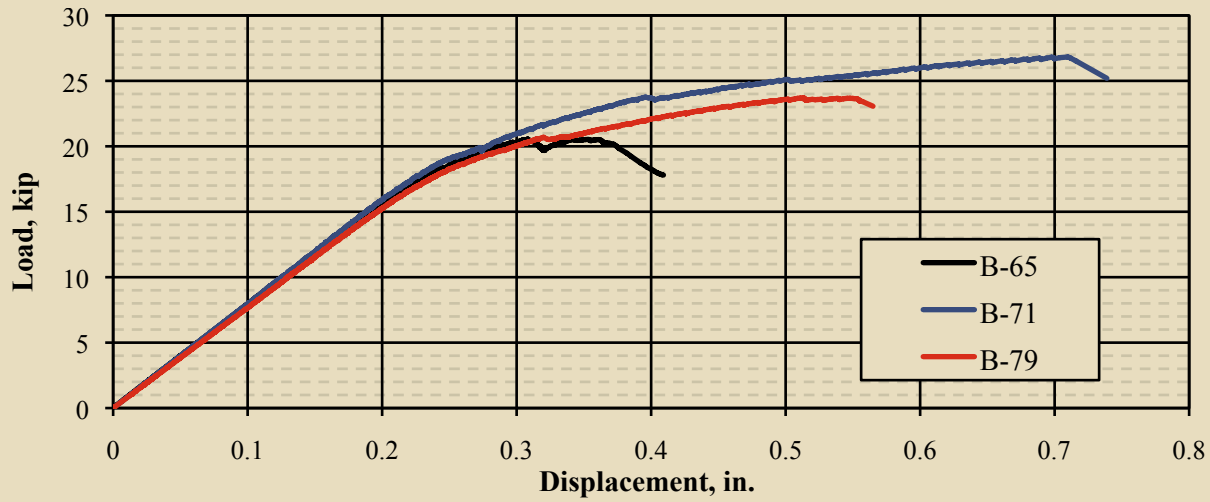

Figure 15. This figure compares the relationship for the ends of the girders with shear reinforcement. Note: 1 in. = 25.4 mm; 1 kip = 4.448 kN.

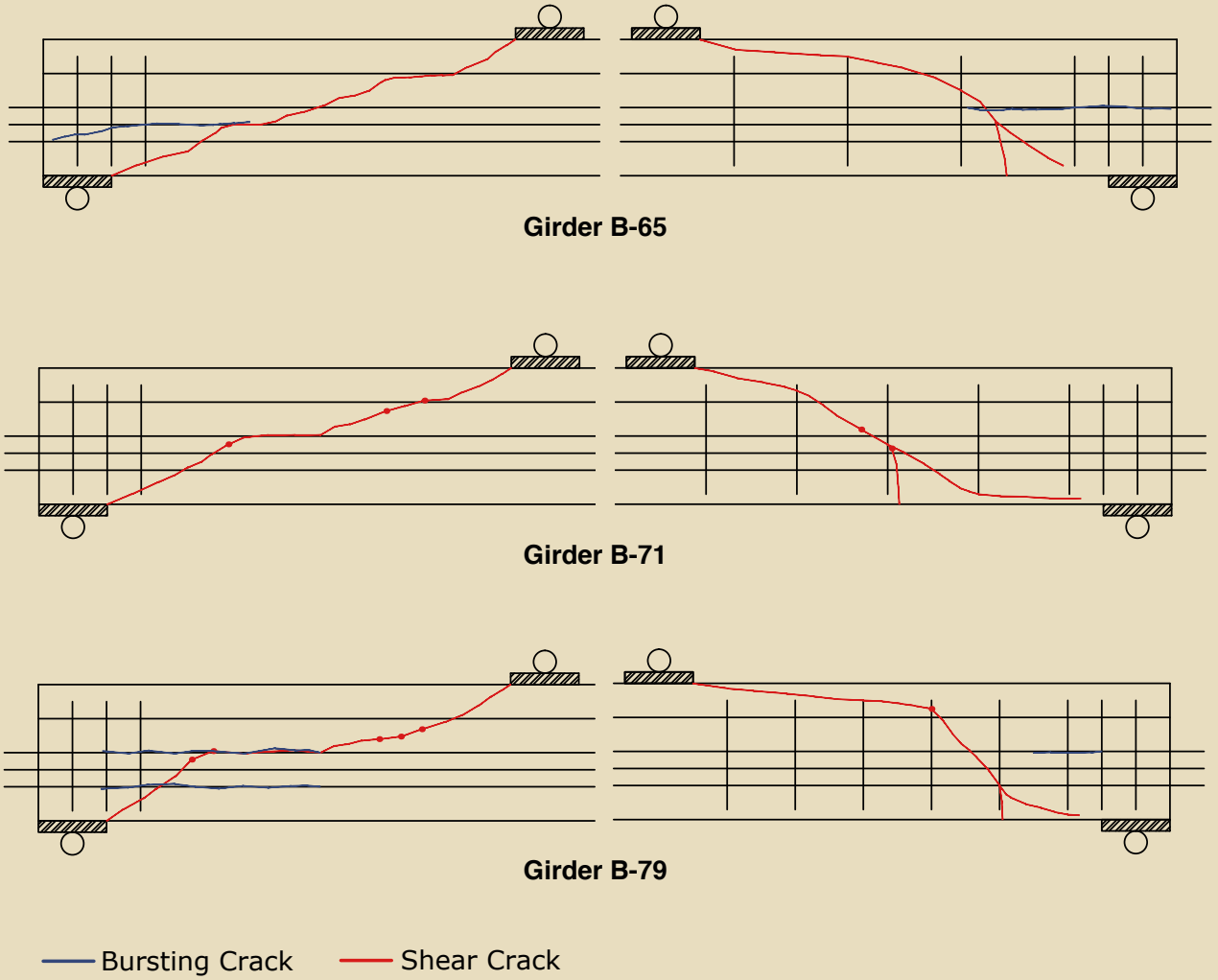

Figure 16. This drawing shows the bursting cracks and shear failure patterns.

- The shear capacity of girders produced using low coarse-aggregate-content SCC is difficult to ascertain. Based on the limited test results presented here, their capacity is well below the capacity predicted using current design equations. Further testing is needed to determine the impact of low coarse aggregate content on the shear performance of SCC girders.

- Girder end-region cracking is of concern due to its impact on shear performance. End-region cracking should be studied in full-scale SCC girders to evaluate the need for further research, particularly if the use of SCC mixtures with reduced aggregate contents is continued to maintain SCC flowability.

Acknowledgments

The authors acknowledge the financial support of Coreslab Structures Inc. in Marshall, Mo., and that of the Center for Transportation Infrastructure and Safety at the Missouri University of Science and Technology (formerly the University of Missouri–Rolla). We also thank the engineers and personnel at Coreslab Structures Inc. for their contributions during planning and production. We are grateful for the technician and staff support from the Center for Infrastructure Engineering Studies and the Department of Civil, Architectural, and Environmental Engineering at the Missouri University of Science and Technology.

References

1. Brewe, J., and J. J. Myers. 2010. High-Strength Self-Consolidating Concrete Girders Subjected to Elevated Compressive Fiber Stresses, Part 1: Prestress Loss and Camber Behavior. *PCI Journal*, V. 55, No. 4 (Fall): pp. 59–77.

2. Liniers, A. D. 1987. Microcracking of Concrete under Compression and Its Influence on Tensile Strength. *Materials and Structures*, V. 20, No. 116 (March): pp. 111–116.

Table 6. Comparison of actual versus predicted shear capacity (no stirrups)

Designation	B-79		B-71		B-65	
Shear failure load, kip	11.7	Ratio*	14.9	Ratio*	18.0	Ratio*
Predicted capacity using predicted losses						
PCI Design Handbook, kip	15.8	1.35	16.2	1.09	16.6	0.93
Response-2000, kip	23.3	1.99	24.3	1.63	25.2	1.41
Predicted capacity using measured losses						
PCI Design Handbook, kip	14.5	1.24	15.3	1.02	15.8	0.88
Response-2000, kip	21.9	1.87	23.4	1.57	24.2	1.35

*Ratio of predicted capacity to measured capacity
Note: 1 kip = 4.45 kN.

Table 7. Comparison of actual versus predicted shear capacity (stirrups)

Designation	B-79		B-71		B-65	
Shear failure load, kip	23.7	Ratio*	26.8	Ratio*	20.6	Ratio*
Predicted capacity using predicted losses						
PCI Design Handbook, kip	32.3	1.36	28.6	1.06	26.5	1.29
Response-2000, kip	31.2	1.32	30.0	1.12	28.3	1.38
Predicted capacity using measured losses						
PCI Design Handbook, kip	31.0	1.31	27.7	1.03	24.7	1.20
Response-2000, kip	30.7	1.29	29.7	1.11	28.5	1.39

*Ratio of predicted capacity to measure capacity
Note: 1 kip = 4.45 kN.

3. Smadi, M. M., and F. O. Slate. 1989. Microcracking of High and Normal Strength Concretes under Short- and Long-Term Loadings. *ACI Materials Journal*, V. 86, No. 2 (March–April): pp. 117–127.

4. Birrcher, D. B., R. G. Tuchscherer, D. Mraz, A. Castro, O. Bayrak, and M. E. Kreger. 2006. Effects of Increasing the Allowable Compressive Release Stress of Pretensioned Girders. In *The PCI National Bridge Conference: Proceedings, October 23–25, 2006, Grapevine, Texas*. CD-ROM.

5. American Association of State Highway and Transportation Officials (AASHTO). 2007. *AASHTO LRFD Bridge Design Specifications*. 4th ed. Washington, DC: AASHTO.

6. ACI Committee 318. 2005. *Building Code Requirements for Structural Concrete (ACI 318-05) and Commentary (ACI 318R-05)*. Farmington Hills, MI: American Concrete Institute (ACI).

7. PCI Industry Handbook Committee. 2004. *PCI Design Handbook: Precast and Prestressed Concrete*. 6th ed. Chicago, IL: PCI.

8. ASTM A416. *Standard Specification for Steel Strand, Uncoated Seven-Wire for Prestressed Concrete*. West Conshohocken, PA: ASTM International.

9. ASTM A615. *Standard Specification for Deformed and Plain Carbon-Steel Bars for Concrete Reinforcement*. West Conshohocken, PA: ASTM International.

10. Collins, M. P., and D. Mitchell. 1991. *Prestressed Concrete Structures.* Prentice-Hall Inc.

11. American Association of State Highway and Transportation Officials (AASHTO). *AASHTO LRFD Bridge Design Specifications—2005 Interim Revisions*. 3rd ed. Washington, DC: AASHTO.

12. Naito, C. J., G. Parent, and G. Brunn. 2006. Performance of Bulb-Tee Girders Made with Self-Consol-

idating Concrete. *PCI Journal*, V. 51, No. 6 (November–December): pp. 72–85.

Notation

a = distance between support and concentrated load

A_c = gross area of concrete section

A_{ci} = area of each individual concrete layer

A_{ps} = area of each layer of prestressing tendons

A_s = area of steel to be placed within a distance of $h/4$ from the end of the member (anchorage zone)

C_c = resultant concrete compressive stress for moment curvature analysis

d_p = distance from top fiber of section to prestressing steel

e_{ps} = prestressing strand eccentricity

f_{ci} = stress at the centroid of each individual concrete layer

f'_{ci} = concrete compressive strength at release of prestressing

f_{pe} = effective prestress after losses

f_r = modulus of rupture of concrete

f_s = steel stress for anchorage zone, not to exceed a maximum working stress of 20 ksi (137 MPa)

h = height of girder

I_g = gross section moment of inertia

M = applied moment

M_{cr} = cracking moment

M_d = dead-load moment

P = applied load

P_{eff} = effective prestressing force after losses

P_r = factored bursting resistance of the anchorage zone

S_b = gross bottom-section modulus

T_s = resultant steel tensile stress for moment-curvature analysis

x = location along member

y_b = distance from neutral axis to bottom fiber of section

y_t = distance from neutral axis to top fiber of section

Δ = midspan displacement

Δx = distance between two points

ϕ = curvature at a specific point

About the authors

Jared E. Brewe, PhD, is an associate II in Structural Engineering and Mechanics for CTLGroup in Skokie, Ill., and a former graduate student in the Department of Civil, Architectural, and Environmental Engineering at Missouri University of Science and Technology in Rolla, Mo.

John J. Myers, PhD, P.E., is an associate professor and interim center director for the CTIS National University Transportation Center in the Department of Civil, Architectural, and Environmental Engineering at Missouri University of Science and Technology in Rolla, Mo.

Synopsis

The design of prestressed concrete members is restricted by the requirement that the extreme compressive fiber stress at midspan be less than 60% of the concrete compressive strength at release of prestressing. The purported purpose of this limit is to provide serviceability performance, but it places unnecessary limits on the capability of the materials. For this research program, six prestressed concrete girders were produced with high-strength, self-consolidating concrete and subjected to elevated compressive fiber stress levels ranging from 65% to 84% of initial concrete compressive strength at release of prestressing. Part 1 of this series analyzed time-dependent prestress losses and camber behavior and compared these values with the results from typical prediction methods. This second part examines the flexural and shear behavior of the same girders. The results of structural testing indicated little reduction in flexural capacity of girders subjected to elevated stress levels, but further testing in shear is needed to reduce the variability in the results. The results reported here suggest that an increase in the allowable compressive stress limit up to at least 70% of the initial concrete compressive strength at release of prestressing at any location is feasible.

Keywords

Allowable release stress, high-strength concrete, modulus of elasticity, prestress transfer, self-consolidating concrete.

Review policy

This paper was reviewed in accordance with the Precast/Prestressed Concrete Institute's peer-review process.

Reader comments

Please address any reader comments to journal@pci.org or Precast/Prestressed Concrete Institute, c/o *PCI Journal*, 200 W. Adams St., Suite 2100, Chicago, IL 60606.